Journal of Power Sources 182 (2008) 370–376

Contents lists available at ScienceDirect

Journal of Power Sources

journal homepage: www.elsevier.com/locate/jpowsour

Light harvesting enhancement for dye-sensitized solar cells by novel anode containing cauliflower-like TiO_2 spheres

Lei Yang[a,b], Yuan Lin[a,*], Jianguang Jia[c], Xurui Xiao[a], Xueping Li[a], Xiaowen Zhou[a]

[a] Beijing National Laboratory for Molecular Science, Key Laboratory of Photochemistry, Institute of Chemistry, Chinese Academy of Sciences, Beijing 100080, PR China
[b] Graduate University of the Chinese Academy of Sciences, Beijing 100049, PR China
[c] Department of Chemistry, School of Science, Beijing University of Chemical Technology, Beijing 100029, PR China

ARTICLE INFO

Article history:
Received 5 December 2007
Received in revised form 6 March 2008
Accepted 10 March 2008
Available online 14 March 2008

Keywords:
Dye-sensitized solar cell
Light scattering effect
Microstructure
Photo-anode
TiO_2

ABSTRACT

Cauliflower-like TiO_2 rough spheres, which are about 200 nm large, have greatly enhanced light harvesting efficiency and energy conversion efficiency of dye-sensitized solar cells (DSC), due to their high light scattering effect and large BET surface area (80.7 $m^2\ g^{-1}$) even after calcinations at 450 °C for 30 min. The large size TiO_2 rough and smooth spheres, produced at different initial temperatures by hydrolysis of $Ti(OBu)_4$ with P105 ($EO_{37}PO_{56}EO_{37}$) or F68 ($EO_{78}PO_{30}EO_{78}$) tri-block copolymer as structural agents, have nearly the same diameter of ~275 nm and strong light scattering effects in the wavelength of 400–750 nm. However, rough spheres have even higher light scattering effect and larger BET surface area than smooth spheres for the roughness of the surface. By adding 25 wt.% large TiO_2 spheres into the over-layer of TiO_2 film composed of ~20 nm TiO_2 particles as light scattering centers, the energy conversion efficiency of the film containing rough spheres reaches 7.36%, much larger than that of smooth spheres (6.25%). From another point of view, the TiO_2 rough spheres may have the satisfying ability in other fields of application such as photo-catalysis, drug carriers and so on.

1. Introduction

Dye-sensitized solar cells (DSC) [1] which are regarded as a new generation photovoltaic devices, have been studied extensively [2–4] due to their high efficiency and low-cost. Traditionally, DSC utilize a porous nanocrystalline TiO_2 film covered with ruthenium-bipyridyl-based dyes which absorb light as the photoelectrode material and triodide/iodide as the redox relay in the electrolyte. With nanocrystalline TiO_2 film, short circuit photocurrent density (J_{sc}) of DSC is chiefly determined by the efficiency of light absorption, charge injection and charge collection [1]. Light absorption efficiency can be enhanced by increasing the dye loading, equivalent optical path and molar extinction coefficient of dye. Moreover, the molar extinction coefficient of certain dye could not be altered.

To enhance the light harvesting capacity of the DSC, especially in the red or near infrared region, both high dye loading and long optical path are needed. Grätzel [1] was the first introduces nanocrystalline TiO_2 films of 10-μm thick, which composed of 15-nm-sized particles, to improve the overall conversion efficiency from less than 1% of single crystal film to 7.1–7.9% due to its 2000-fold large in surface area. Since then, many researchers have made efforts to increase surface area, for example, prepared high ordered structures with template [5,6], decreased the size of the TiO_2 to 3–5 nm [7], and optimized the film thickness [8]. However, theoretical calculations demonstrate that the amount of dye adsorption reaches maximum and roughness factor is 1500 with particle size of 5–10 nm [9], accounting of average diameter of dye with 1 nm. Grätzel has optimized the thickness of TiO_2 film electrode between 8 and 12 μm [10]. Conversion efficiency decreases with film thickness larger than 12 μm, even though it has larger specific surface area, because the increase of film thickness will go against the electrolyte diffusion and electron transport, which compensate the positive effect of the increase of specific surface area.

Optical confinement [11] and light scattering effect [12] are found to be necessary and effective for the solar cells to improve the light absorption efficiency by increasing the equivalent optical path. It has been proved that the application of light scattering remarkably improves the light absorption efficiency of the dye in long wavelength region, not only in theoretical simulations [13] but also in experimental studies [14]. In previous works, around three types of scattering centers, large particles [15,16], scattering spherical voids in nanocrystalline TiO_2 films by sacrificing polystyrene (PS) spheres [17], and highly ordered TiO_2 nanotube arrays [18],

* Corresponding author. Tel.: +86 10 82615031; fax: ++86 10 82617315.
E-mail address: linyuan@iccas.ac.cn (Y. Lin).

0378-7753/$ – see front matter © 2008 Elsevier B.V. All rights reserved.
doi:10.1016/j.jpowsour.2008.03.013

are effective and available to enhance light scattering effect so as to the light absorption efficiency. For the optimal scattering effect, the diameter of scattering centers should be near half of light wavelength according to Mie theory and around 200–400 nm [19].

The application of pure large particles could hardly receive the best effect, as large particles decrease effective surface area. In order to improve the DSC performance, the advantage of high surface area of small particle (5–10 nm) and the strong light scattering effect of large particle (200–400 nm) must be combined. Multilayer structure including active layer composed of small (<50 nm) TiO_2 particles and scattering layer all composed of large particles (>500 nm) was investigated in DSC [12] and it improved the conversion efficiency to 6.8%. Further, a more sophisticated multilayer structure with gradually increased particle size from the innermost layer to the outer layer deserved to be constructed and tested [20]. Another is a colligation, which has combined different scattering centers, different ratios and multilayer structures in expectation of having the best light scattering effect. In this idea, Dai and coworkers [21] have designed photoelectrodes with multilayer ($\geq$3 layers) structure containing small pore sized films, larger pore sized films, and light-scattering particle films on the conducting glass with a desirable thickness to balance the two conflict factors which involved light scattering effect and specific surface area.

However, for smooth spherical or cubic particles, the conflict between specific surface area and light scattering effect cannot be preferably solved. In this regard, we designed a new type of particle with size of 200–400 nm as scattering centers and rough surface which kept large surface area and strong light scattering effect to meet our purpose.

Neutral non-ionic surfactants and block copolymers are indeed interesting as supramolecular templates which have brought TiO_2 thin films highly organized nanotexture [22], hexagonal pore structures [23,24], and high specific surface areas [25]. They also used to prepare mesoporous materials, because they are capable of imparting larger pores and thicker walls, and hazard-free, and easy to be removed from the mineral framework [26].

Cauliflower-like TiO_2 rough spheres which have both large specific surface area and strong light scattering effect were synthesized from hydrolysis of $Ti(OBu)_4$ by using tri-block copolymer as template [27]. The energy conversion efficiency of the photo-anode made from rough TiO_2 spheres is up to 7.36%, 1.11% higher than that of smooth ones.

2. Experimental

2.1. Chemicals

Organic solvents (acetone, absolute ethanol), ethylene glycol (EG) and $Ti(OBu)_4$ (TBT) were purchased from Beijing Chemical Industry Group Imp. & Exp. Co., China, and used without further treatment. Doubly distilled water was also used as a solvent. Pluronic P105 (BASF) is a poly(ethyleneoxide)–poly(propy1eneoxide)–poly(ethy1ene oxide) (PEO–PPO–PEO) triblock copolymer with a nominal molecular weight of 6500, and it can be represented by the chemical formula $EO_{37}PO_{56}EO_{37}$. F68 (Aldrich) has a nominal molecular weight of 8400 and can be represented by the chemical formula $EO_{78}PO_{30}EO_{78}$.

2.2. Synthesis of cauliflower-like TiO_2 rough spheres and comparison materials

In a typical synthesis, two solutions were prepared. First, 1.5 ml $Ti(OBu)_4$ (TBT) was added to 25 ml ethylene glycol(EG). The solution (named as A) was covered with a plastic membrane and magnetically stirred for 6 h at room temperature, and was then kept at −4 °C (or 50 °C) for 1 h. Secondly, an acetone bath (named as B) containing a small amount of aqueous Pluronic P105 (or F68) copolymer solution (~0.35–0.5 ml) was kept at the same temperature as solution A under vigorous stirring for 2 h, and then solution A was poured into solution B. After aging for 1 h, the white precipitate was harvested by centrifugation. Next, the particles were washed with doubly distilled water and ethanol several times to remove EG and other impurities from the surfaces of the titania hybrid particles. Then, the as-synthesized TiO_2 samples were dried in the oven under vacuum at room temperature. TiO_2 smooth spheres can be produced in the same way, only demanding F68 for template.

Titanium(IV) isopropoxide (Aldrich, 98%) was used as the precursors and mixed with pH 2 acetic acid solutions and hydrolysis at 80 °C and then autoclaved at 230 °C to prepare small particles (~20 nm) colloidal TiO_2 suspension with an appropriate viscosity [28].

2.3. Fabrication of DSC

DSC were fabricated as detailed elsewhere [29]. Transparent layers of the films were fabricated via doctor-blade technique using a paste of TiO_2 nanoparticles (NP for short) on a transparent conducting glass (TCO) substrate. In order to improve the interconnection between TiO_2 rough or smooth spheres (RS or SS for short), scattering layers composed of RS or SS and ~20 nm TiO_2 NP in different proportions were dispersed in terpineol with ethyl cellulose as a binder and were deposited onto transparent layers using a screen printing method. Then the films were sintered at 450 °C for 30 min.

The TiO_2 nanocrystalline electrode was immersed overnight in a solution of ruthenium dye (ruthenium(2,2′-bipyridyl-4,4′-dicarboxilate)$_2$(NCS)$_2$ that was dissolved in ethanol) (concentration of 3×10^{-4} M). One drop of an iodine-based electrolyte solution was deposited onto the surface of the electrode and penetrated inside the TiO_2 film via capillary action. The electrolyte solution was composed of 0.05 mol l^{-1} of iodine(I_2), 0.5 mol l^{-1} lithium iodide (LiI), and 0.05 mol l^{-1} *tert*-butylpyridine (Aldrich) that was dissolved in 3-methoxypropionitrile (all the chemicals except *tert*-butylpyridine were purchased from Acros Chemical). A platinized counter electrode was then clipped onto the top of the TiO_2 working electrode to form the test cell.

2.4. Characterization

The morphology was examined by scanning electron microscopy (SEM, S-4300F, Hitchi, 15 kV). The crystallinity and phase-purity of the products were studied by X-ray powder diffraction (XRD) using a Riguku D/max 2500 and Cu Kα irradiation. A Surface Area and Porosity Analyzer (ASAP 2020) was used to analyse the mesoporous structure of as-synthesized particles. Diffuse reflection was measured in the 300–800 nm wavelength range on Model U-3010 spectrophotometer (HITACHI) with Integrating Sphere as accessory. The sphere as well as the reference plates is coated with $BaSO_4$. A tungsten lamp was used as the light source together with a grating monochromator and a photomultiplier detector. The scanning speed was 2 nm s^{-1}. Photoelectrochemical measurements were recorded with a PAR potentiostat (Model 273) under the irradiation of 100 mW cm^{-2} from a 500 W xenon lamp, and the active area was 0.2 cm^2. IPCE plotted as a function of excitation wavelength, were recorded on a Model SpectraPro-300i Meter Triple Grating Monochromator/Spectrograph (Acton Research Corporation) under the irradiation of a 500 W xenon lamp.

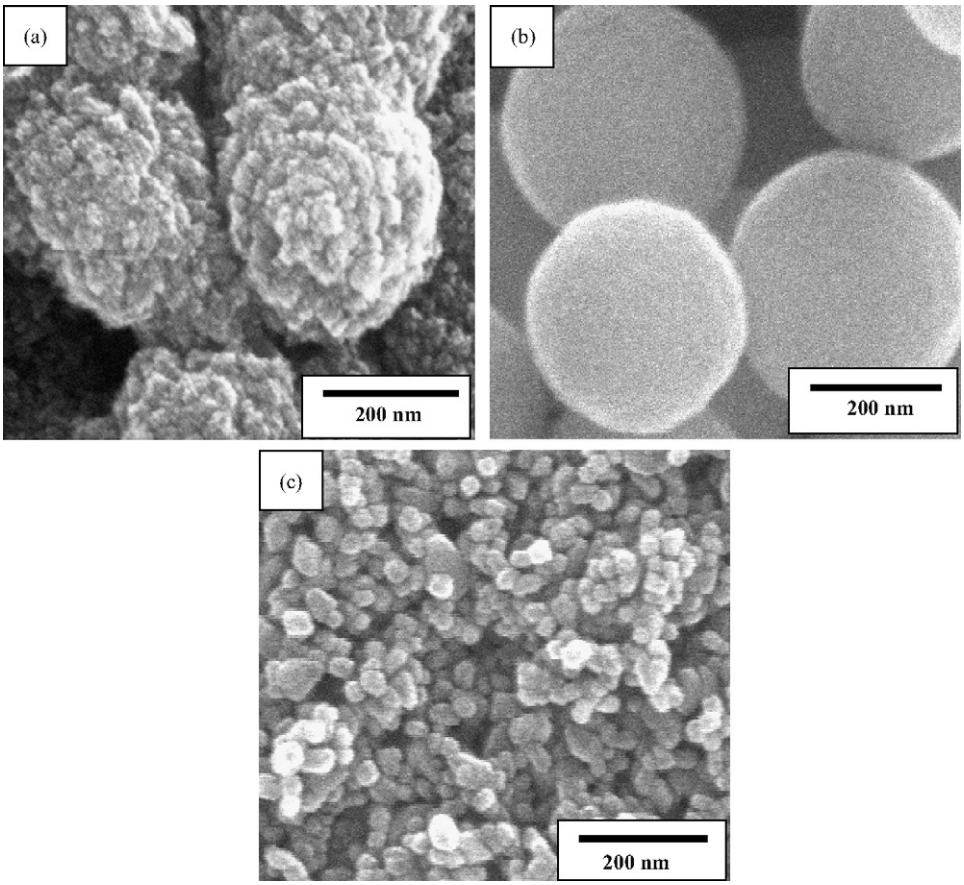

Fig. 1. SEM images of TiO_2 samples: (a) rough spheres (RS for short); (b) smooth spheres (SS for short); (c) nanoparticles (NP for short). The mean diameters of these colloids were ~275 nm, ~272 nm and ~20 nm, respectively (evaluation of more than 40 particles).

3. Results and discussion

3.1. Morphology and phase transfer of TiO_2 materials

The present study explores a simple procedure to generate cauliflower-like TiO_2 rough spheres (RS) by P105, and the morphology has been examined by scanning electron microscopy (SEM), as shown in Fig. 1a. For comparison, TiO_2 smooth spheres (SS) (by F68) shown in Fig. 1b have nearly the same size as the rough spheres [27]. TiO_2 nanopaticles (NP, Fig. 1c) of 10–20 nm have been extensively used in DSC since 1991 [1], and been proven to have high dye loading and the overall conversion efficiency of the solar cells.

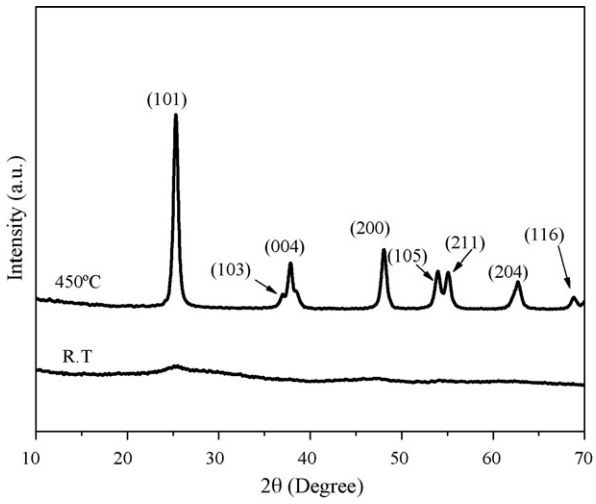

Fig. 2. XRD spectrum of sample RS showing the formation of various phases at two different temperatures: amorphous (RT), anatase (450 °C).

X-ray diffraction (XRD) patterns (Fig. 2) were taken from sample RS before and after it was annealed at 450 °C for 30 min. It's clear from the results that the as-synthesized spheres are amorphous without any diffraction peaks. After calcinations at 450 °C for 30 min, the phase transferred to pure anatase, which are consistent with previously reported results [30]. Sample SS is the same.

3.2. Surface roughness—larger scattering effect in DSC application

As shown in Table 1, R100 has better photoelectrochemical performance than S100. Compared to R0, R100 has even higher J_{sc} with much lower dye loading due to the scattering effect by rough spheres in DSC. For S100, small dye loading could be mostly due to the decrease of the surface area of smooth spheres. As a result, the J_{sc} of S100 is much lower. On account of the same FT for R100 and S100, we can conclude that the increase of dye loading may largely owe to rough surface of the rough spheres. Besides, V_{oc} of R100 was ~40 mV larger than that of S100. This is probably related to the good light scattering effect caused by TiO_2 rough spheres.

Light scattering effect was investigated by diffuse reflection (R_d) spectrum. When a beam of light irradiated on a sample, it is reflected, scattered and transmitted through the sample material. The part of the beam that is scattered within a sample and returned to the surface is considered to be diffuse reflection. Scattering of particles increases the contribution of the diffuse reflection com-

Table 1
Photovoltaic characteristic for different layer structures, TiO_2 nanocrystalline films with first layers composed of NP and scattering layers composed of a mixture of TiO_2 RS or SS and NP in different ratios

Device	Dye loading ($\times 10^{-7}$ mol cm^{-2})	J_{sc} (mA cm^{-2})	V_{oc} (V)	FF (%)	η (%)	FT[a] (μm)
R100	0.593	15.9	0.706	58.4	6.56	8.1
S100	0.398	13.8	0.664	59.0	5.43	8.1
R0	0.906	15.6	0.651	63.2	6.39	8.2

R100, S100 and R0 represent the over layers were composed of pure TiO_2 RS, SS and NP, respectively, they were measured under illumination with AM 1.5 simulated sunlight. The symbols Dye loading, J_{sc}, V_{oc}, FF, and η represent the amount of dye adsorption, short-circuit photocurrent density, open-circuit voltage, fill factor, and solar-energy-conversion efficiency, respectively.

[a] FT represents the thickness of TiO_2 nanocrystalline film.

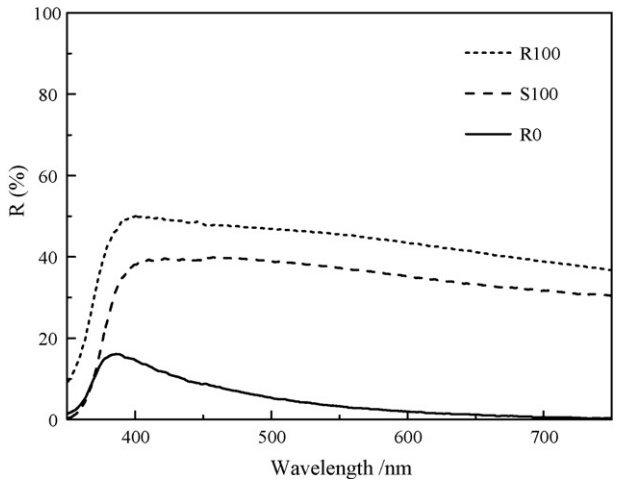

Fig. 3. Diffuse reflection (R_d) of TiO_2 nanocrystalline films with first layers composed of NP and scattering layers composed of a mixture of TiO_2 RS or SS and NP in different ratios. R100, S100 and R0 represent the over layers were composed of pure TiO_2 RS, SS and NP, respectively, which have been sintered at 450 °C for 30 min.

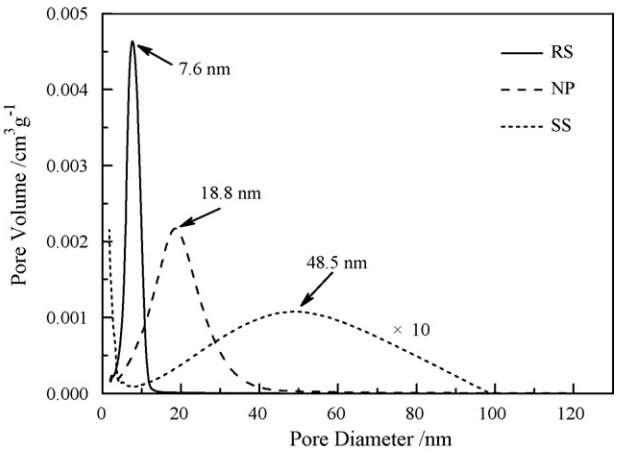

Fig. 4. BJH pore size distribution plot of TiO_2 samples RS, SS and NP.

ponent in the spectrum. As shown in Fig. 3, both R100 and S100 have higher diffuse reflection capacities than that of R0 ranging from 400 nm to 750 nm. R0 represents that the film is composed of two layers of NP in ~20 nm size, so the diffuse reflection to light decreased rapidly with the increase of the wavelength. R_d value of R100 is above S100 even at short wavelength of 350 nm, as well as in the whole visible spectrum. Because of the diameters of both RS and SS were nearly the same, the results above implied that rough surface may have great contribution to the diffuse reflection in the visible light region. However, the effect of surface roughness on scattering cannot be considered independently of the host particle. Rather, the effectiveness of surface roughness to affect scattering depends on the particle size [31].

3.3. Microstructure of cauliflower-like TiO_2 rough spheres

Table 2 summarizes the BET surface areas and average pore diameters of RS, SS and NP after calcinations. For the sample RS, the surface area was up to 80.7 m^2 g^{-1} and an average pore diameter of 7.3 nm was measured. The surface area of SS was only 9.14 m^2 g^{-1}, but average pore diameter was up to 25.7 nm. NP sample have a normal results, with a surface area of 66.5 m^2 g^{-1} and an average pore diameter of 15.4 nm.

Table 2
BET surface areas of three TiO_2 samples sintered at 450 °C for 30 min

Samples	BET Surface Area (m^2 g^{-1})	Average Pore Diameter (nm)
RS	80.7	7.30
SS	9.14	25.7
NP	66.5	15.4

To all appearances in Fig. 4, two different kinds of curves were seen. First, pore volumes drop abruptly at ~3 nm, which indicates that sample SS has pores less than 5 nm size inside, and the broad lower peak of SS at ~48.5 nm represents the voids between the TiO_2 aggregates. Second, the curves of the RS and NP samples have evident peaks, indicating that pore diameters of the two samples have concentrated between 5–10 nm and 10–30 nm, respectively. Because the size of NP is ~20 nm, so the 18.8 nm pore diameter at the peak represents the voids between NP aggregates. However, the peak of RS are not only resulted from rough surfaces of RS abut against each other, due to the surface protuberance which relates to the formation of pores between RS, but also may represent the pores inside the RS.

3.4. Surface roughness—more dye loading in optimal microstructure

In order to optimize the results and to find the different inconsistency between BET surface area of RS and dye loading of R100, we prepared double layer film electrodes made up of a transparent layer containing 20 nm sized NP and a scattering layer composed of a mixture of TiO_2 materials RS and NP at different molar ratio, defined as R0, R25, R50, and R100, respectively, and investigated through SEM, R_d, IPCE and *I–V* characterization.

Fig. 5 shows the surface morphology of TiO_2 photoelectrodes with four different structures which have the same transparent layers all composed of NP, and the scattering layers composed of different ratios of RS/NP mixtures. We could see that R25 and R50 films have the good connections between RS and NP, while R100 film has poor connections due to the large spacing between scattering particles. By way of studying which assembled electrode has a good balance between interconnections, dye loading and light scattering effect, we measured cell performances for the four electrodes under illumination with AM 1.5 simulated sunlight.

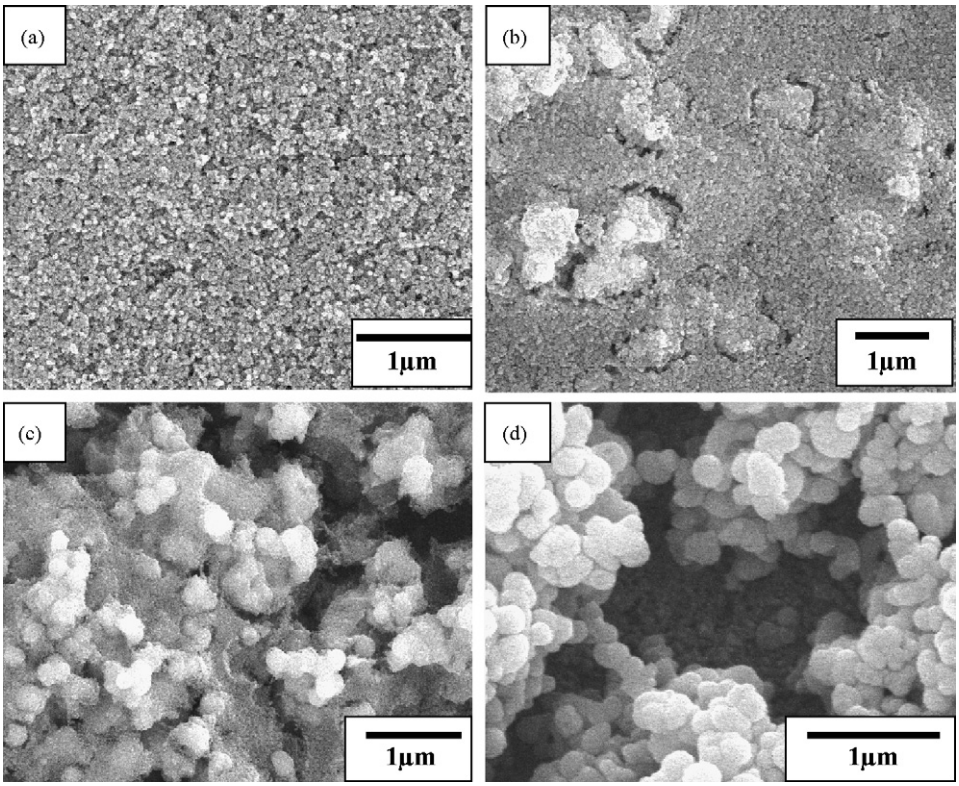

Fig. 5. SEM image of TiO_2 nanocrystalline films with first layers composed of NP and scattering layers composed of TiO_2 RS of (a) 0 wt.%, R0; (b) 25 wt.%, R25; (c) 50 wt.%, R50; (d) 100 wt.%, R100, which have been sintered at 450 °C for 30 min.

It can be seen from Table 3 that RS/NP ratios have a significant influence on the performance of these electrodes in DSC. For comparison, S25 is prepared by mixing 25% SS with 75% NP as the scattering layer. First, *dye loadings* of the electrodes in *R* series decreased with the increase of the RS/NP ratio although the surface area of the RS (80.7 $m^2 g^{-1}$) was larger than NP (66.5 $m^2 g^{-1}$). An explanation we would give for this conflict between *dye loading* and surface area was that the surface area was from surfaces of the material and pores inside it, currently the pore diameters of RS are small and partially airtight, as a result, high surface area of RS has not been in full use; besides, the SEM (Fig. 5) images clearly showed that the porosities of the four electrodes increased a lot with the increase of the RS/NP ratio, which also results in the decrease of the *dye loadings*. For S25, small dye loading could be mostly due to the decrease of the surface area of smooth spheres. Second, the rate of dye using (RDU) which can be described as the using efficiency of adsorbed dyes increased with the amounts of RS added to the films, and in R25 was larger than that of S25. Both *dye loading* and RDU opened out the tendency of J_{sc}, which greatly influenced

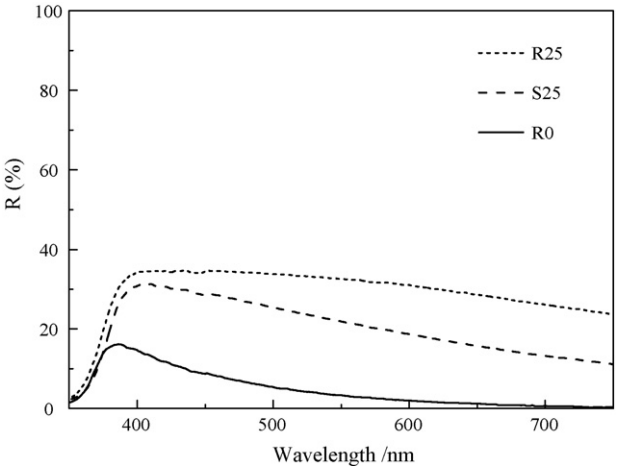

Fig. 6. Diffuse reflection (R_d) of different layer structures denoted as R25, S25 and R0.

Table 3
Photovoltaic characteristics for different layer structures, they were measured under illumination with AM 1.5 simulated sunlight

Device	FT[a] (μm)	Dye loading ($\times 10^{-7}$ mol cm^{-2})	J_{sc} (mA cm^{-2})	RDU[b] ($\times 10^7$ mA mol^{-1})	V_{oc} (V)	FF (%)	η (%)
R0	8.2	0.906	15.6	17.2	0.651	63.2	6.39
R25	8.1	0.775	18.1	23.4	0.671	60.6	7.36
R50	8.0	0.686	16.6	24.2	0.699	58.3	6.76
R100	8.1	0.593	15.9	26.8	0.706	58.4	6.56
S25	8.1	0.657	14.4	21.9	0.696	62.1	6.25

The symbols Dye loading, J_{sc}, V_{oc}, FF, and η represent the amount of dye adsorbed by the films, short-circuit photocurrent density, open-circuit voltage, fill factor, and solar-energy-conversion efficiency, respectively.

[a] FT represents the thickness of TiO_2 nanocrystalline film.

[b] RDU represents the rate of dye using, result from J_{sc}/Dye loading.

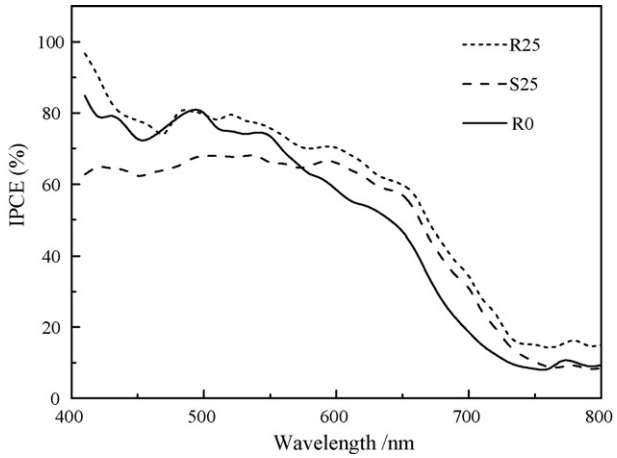

Fig. 7. Incident-photon-to-current conversion efficiency (IPCE) curves of photoelectrical performance with R25, S25 and R0 electrodes.

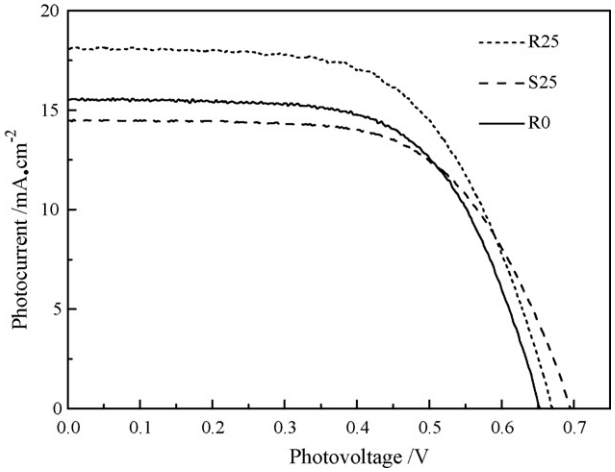

Fig. 8. *I–V* curves of device R25 (short dashed line), S25 (dashed line) and R0 (solid line) at air mass 1.5 (100 mW cm^{-2}) illumination.

by surface area and light scattering effect of the film. R25 has the largest J_{sc}, which is due to the good balance between *dye loading* and RDU. The efficiencies (η) of the electrodes were in accordance with J_{sc}, and the highest efficiency of 7.36% was obtained when RS was at 25 wt.%, while the η of R0, R50 and R100 were much lower, as 6.39%, 6.76% and 6.56%, respectively.

As shown in Fig. 6, with 25% of TiO_2 large spheres, both R25 and S25 have higher R_d values than that of R0 ranging from 400 nm to 750 nm. Further more, at short wavelengths, R_d values are nearly the same for both R25 and S25, whereas at $\lambda > 400$ nm they differ a lot. R_d value of S25 is decreased from 35% to 10% and the curve of R25 declines a little along with the increase of wavelength ranging from 400 nm to 750 nm. The largest difference between the two R_d values is ~13%, which is from around 550 nm to 750 nm. Due to the diameters of both RS and SS were nearly the same, we can clearly pick up the contribution of rough surface to the diffuse reflection in the visible light, which are consistent with previously result above.

3.5. Incident-photon-to-current conversion efficiency

For the sake of investigating the definite effect on light absorption efficiency due to the light scattering effect mentioned above, we introduced the incident-photo-to-current conversion efficiency (IPCE), which is defined as the ratio of collected electrons to incident photons. It is clearly showed in Fig. 7 that the IPCE values of R25, S25 and R0 are larger than 60% over a large part of the visible light region. The dramatic decrease in IPCE from 550 nm to longer wavelength is ascribed from the low absorption of N3 in the red region, the nano-film is transparent and has no light scattering, light loss due to the transmittance of light with wavelength greater than 600 nm accounts for the poor IPCE in the red region [20]. Compared to the IPCE value of R0, the decrease in IPCE at short wavelengths of S25 could be mainly due to the decrease of the surface area so as to the dye loading (0.657×10^{-7} mol cm^{-2} for S25, 0.906×10^{-7} mol cm^{-2} for R0). However, the IPCE values in the red region (570–750 nm) of S25 were higher than that of R0, which is in accordance with the light scattering effect of large TiO_2 spheres. And the increase in IPCE of R25 in the full region (400–800 nm) could be due to the less decrease of the dye loading (0.775×10^{-7} mol cm^{-2}) and much more increase of the light scattering effect. The results confirmed that the light scattering effects of RS and SS increased the absorption of N3 in the red region. Moreover, rough spheres were more effective to enhance the light harvesting capacity of the DSC and without any decrease in IPCE at short wavelengths due to their rough surface scattering and large surface area.

I–V characteristics as shown in Fig. 8 clearly recorded the advances of R25. Both J_{sc} and V_{oc} were increased a lot in case of adding RS to the nanocrystalline films, so as to the large increase of η. For SS, a large increase of V_{oc} accompanied with a sharp decrease of J_{sc}, resulted in the η falling from 6.39% to 6.25%.

The results confirmed that light scattering effect for both rough surfaces and sizes and large BET surface area of the large TiO_2 rough spheres have greatly impacted on the light harvesting capacity in DSC. From another point of view, the as synthesized TiO_2 rough spheres may have the satisfying ability in other fields of application such as photo-catalysis, carriers and so on.

4. Conclusions

This paper presents a strategy to enhance the conversion efficiency of DSC when the as synthesized TiO_2 rough spheres were used. TiO_2 rough spheres have greatly enhanced the scattering effect so as to the light harvesting efficiency of the photoanode, and increased J_{sc} with a little decrease of the *dye loading*. Moreover, the *dye loading* of R25 was 0.775×10^{-7} mol cm^{-2}, by ~36.7% higher than that of S25. Via contrasting RS and SS in diffuse reflection, we can conclude that the rough surfaces of the rough spheres have great contribution to the light scattering effect. The overall conversion efficiency of R25 reached 7.36%, over one percentage higher than that of S25 (6.25%).

Supporting information

Fig. 9 shows that the morphology of rough TiO_2 spheres is completely maintained, without collapse. In our experiment, all the titania materials were firstly calcined at 330 °C for 30 min in inert gases atmosphere, and then at 450 °C for 30 min in air to remove the carbides of surfactants and to form anatase phase.

The N_2 adsorption–desorption isotherm of calcined mesoporous titania are shown in Fig. 10. For RS, type IV isotherm is observed, which indicates the mesoporosity. No tailing upward at higher relative pressure shows the formation of long-range order mesoporosity without any contribution of large pores beyond mesopore scale (>50 nm) [32]. In other curves, similar tailing upwards at higher relative pressure show the formation of long-range order

mesoporosity with some contribution of large pores beyond mesopore scale.

Acknowledgments

This work was performed with financial support from National Natural Science Foundation of China (20373075 and 50221201) and National Research Fund for Fundamental Key Project (2006CB202605).

Appendix A. Supplementary data

Supplementary data associated with this article can be found, in the online version, at doi:10.1016/j.jpowsour.2008.03.013.

References

[1] B. O'Regan, M. Graetzel, Nature 353 (1991) 737.
[2] J.T. Jiu, S. Isoda, F.M. Wang, M. Adachi, J. Phys. Chem. B 110 (2006) 2087–2092.
[3] A. Hagfeldt, M. Gratzel, Chem. Rev. 95 (1995) 49.
[4] Y. Chiba, A. Islam, Y. Watanabe, R. Komiya, N. Koide, L.Y. Han, Jpn. J. Appl. Phys. 45 (2006) L638.
[5] M.D. Wei, Y. Konishi, H.S. Zhou, M. Yanagida, H. Sugihara, H. Arakawa, J. Mater. Chem. 16 (2006) 1287–1293.
[6] Y.Q. Wang, S.G. Chen, X.H. Tang, O. Palchik, A. Zaban, Y. Koltypin, A. Gedanken, J. Mater. Chem. 11 (2001) 521–526.
[7] J.T. Jiu, S.J. Isoda, M. Adachi, F. Wang, J. Photochem. Photobiol. A: Chem. 189 (2007) 314–321.
[8] S. Ito, S.M. Zakeeruddin, R.H. Baker, P. Liska, R. Charvet, P. Comte, M.K. Nazeeruddin, P. Péchy, M. Takata, H. Miura, S. Uchida, M. Grätzel, Adv. Mater. 18 (2006) 1202–1205.
[9] J. Ferber, J. Luther, Solar Energy Mater. Solar Cells 54 (1998) 265–275.
[10] M.K. Nazeeruddin, A. Kay, I. Rodicio, R. Humphrybaker, E. Muller, P. Liska, N. Vlachopoulos, M. Gratzel, J. Am. Chem. Soc. 115 (1993) 6382.
[11] A. Usami, Solar Energy Mater. Solar Cells 64 (2000) 73–83.
[12] S. Hore, C. Vetter, R. Kern, H. Smit, A. Hinsch, Solar Energy Mater. Solar Cells 90 (2006) 1176–1188.
[13] Y. Lin, Y.T. Ma, L. Yang, X.R. Xiao, X.W. Zhou, X.P. Li, J. Electroanal. Chem. 588 (2006) 51–58.
[14] (a) S. Hore, C. Vetter, R. Kern, H. Smitc, A. Hinscha, Solar Energy Mater. Solar Cells 90 (2006) 1176–1188;
(b) K. Asagoe, S. Ngamsinlapasathian, Y. Suzuki, S. Yoshikawa, Central Eur. J. Chem. 5 (2007) 605–619.
[15] M. Gratzel, Curr. Appl. Phys., 6S1 (2006) e2–e7.
[16] A.G. Agrios, I. Cesar, P. Comte, M.K. Nazeeruddin, M. Gratzel, Chem. Mater. 18 (2006) 5395–5397.
[17] S. Hore, P. Nitz, C. Vetter, C. Prahl, M. Niggemann, R. Kern, Chem. Commun. (2005) 2011–2013.
[18] G.K. Mor, K. Shankar, M. Paulose, O.K. Varghese, C.A. Grimes, Nano Lett. 6 (2006) 215–218.
[19] W.E. Vargas, G.A. Niklasson, Solar Energy Mater. Solar Cells 69 (2001) 147–163.
[20] Z.S. Wang, H. Kawauchi, T. Kashima, H. Arakawa, Coord. Chem. Rev. 248 (2004) 1381.
[21] L.H. Hu, S.Y. Dai, J. Weng, S.F. Xiao, Y.F. Sui, Y. Huang, S.H. Chen, F.T. Kong, X. Pan, L.Y. Liang, K.J. Wang, J. Phys. Chem. B 111 (2007) 358–362.
[22] M. Zukalova, A. Zukal, L. Kavan, M.K. Nazeeruddin, P. Liska, M. Gratzel, Nano Lett. 5 (2005) 1789.
[23] Hui-Suk, K. Miyazawa, H.S. Zhou, I. Honma, M. Kuwabara, Adv. Mater. 13 (2001) 1377.
[24] S.Y. Choi, M. Mamak, N. Coombs, N. Chopra, G.A. Ozin, Adv. Funct. Mater. 14 (2004) 335.
[25] G. Calleja, D.P. Serrano, R. Sanz, P. Pizarro, Ahitana, Ind. Eng. Chem. Res. 43 (2004) 2485–2492.
[26] G.J. Soler-Illia, E.L. Crepaldi, D. Grosso, C. Sanchez, Curr. Opin. Colloid Interface Sci. 8 (2003) 109–126.
[27] L. Yang, Y. Lin, J.G. Jia, X.P. Li, X.R. Xiao, X.W. Zhou, Micropor. Mesopor. Mater. 112 (2008) 45–52.
[28] Y.T. Ma, Y. Lin, X.R. Xiao, X.P. Li, X.W. Zhou, Chin. Sci. Bull. 50 (2005) 1985.
[29] C.N. Zhang, M. Wang, X.W. Zhou, Y. Lin, S.B. Fang, X.P. Li, X.R. Xiao, K. Cen, Chin. Sci. Bull. 49 (2004) 2033–2036.
[30] X.C. Jiang, T. Herricks, Y.N. Xia, Adv. Mater. 15 (2003) 1205–1209.
[31] T. Nousiainena, K. Muinonenb, J. Quant. Spectrosc. Radiat. Transfer 106 (2007) 389–397.
[32] S.J. Gregg, K.S.W. Sing, Adsorption Surface Area and Porosity, second ed., Academic Press, London, 1982.